

Isofrequency pairing of spinning particles in Schwarzschild-de Sitter spacetime

Daniela Kunst,^{1,*} Volker Perlick,^{1,†} and Claus Lämmerzahl^{1,2,‡}

¹ZARM, University of Bremen, Am Fallturm, 28359 Bremen, Germany

²Institute for Physics, University Oldenburg, 26111 Oldenburg, Germany

It has been established in Schwarzschild spacetime (and more generally in Kerr spacetime) that pairs of geometrically different timelike geodesics with the same radial and azimuthal frequencies exist in the strong field regime. The occurrence of this so-called isofrequency pairing is of relevance in view of gravitational-wave observations. In this paper we generalize the results on isofrequency pairing in two directions. Firstly, we allow for a (positive) cosmological constant, i.e., we replace the Schwarzschild spacetime with the Schwarzschild-de Sitter spacetime. Secondly, we consider not only spinless test-particles (i.e., timelike geodesics) but also test-particles with spin. In the latter case we restrict to the case that the motion is in the equatorial plane with the spin perpendicular to this plane. We find that the cosmological constant as well as the spin have distinct impacts on the description of bound motion in the frequency domain.

PACS numbers:

Keywords:

1. INTRODUCTION

The occurrence of *isofrequency pairs* in the strong field regime of the Schwarzschild spacetime was noticed only recently by Barack and Sago [1]. It says that bound orbits, for which both the radial and the azimuthal motion are periodic, are not uniquely characterized by their frequencies. More precisely, there exist geometrically distinct orbits in the strong field regime that possess the same frequency pairs.

At first, this degeneracy feature may not be much of a surprise. After all, it is known from Newtonian Mechanics that the frequencies of the Kepler ellipses are all degenerate, i.e. the radial and azimuthal frequencies have the same value. This is the reason why the orbits in Newtonian physics are closed.

When general relativistic effects are considered, though, one major difference to Newtonian physics is the periastron shift of bound orbits which are no longer closed. This manifests itself in the non-degeneracy of the frequencies. In the Schwarzschild spacetime we have two independent orbital frequencies, for the radial and for the azimuthal motion. It was long thought that these two frequencies provide another unique parametrization of the orbits, as an alternative to the ones already known, such as the energy and the angular momentum or the periastron and the apastron. However, Barack and Sago [1] showed that in the strong field of Schwarzschild spacetime, i.e. in the highly relativistic regime, there exist pairs of timelike geodesics which are described by the same frequencies. In a follow-up study, Warburton, Barack and Sago [2] generalized the isofrequency pairing to the Kerr geometry. In contrast to the Schwarzschild

case, timelike geodesics in the Kerr spacetime have three degrees of freedom and in their study Warburton et al. found even triperiodic partners. As outlined in Refs. [1, 2], the occurrence of isofrequency pairing is of relevance in view of gravitational wave analysis because it implies that, for the case of an Extreme Mass Ratio Inspiral (EMRI), from the observation of the fundamental frequencies one cannot uniquely determine the shape of the orbit. Shortly after Refs. [1, 2] had appeared, Shaymatov, Atamurotov and Ahmedov [3] investigated the influence of a magnetic field on the orbital frequencies of a charged particle moving in Schwarzschild spacetime and found that the region where isofrequency pairing occurs shrinks for high values of the magnetic field.

In this paper we generalize the results on Schwarzschild isofrequency pairing in two different directions. Firstly, we consider the Schwarzschild-de Sitter spacetime, which is the unique spherically symmetric and static solution to Einstein's vacuum field equations with a positive cosmological constant. Secondly, we consider not only spinless but also spinning test particles. We restrict to the case that the particle moves in the equatorial plane, with the spin perpendicular to this plane. Properties of the Schwarzschild-de Sitter spacetime have been discussed, e.g., in [4–6], and the motion of non-spinning test-particles in this spacetime has been investigated, e.g., in [7–9]. For spinning particles we have to consider the equations of Mathisson-Papapetrou-Dixon [10–12]. As this set of equations is not closed in the sense that there are less equations than variables, an additional condition is needed, usually referred to as a spin supplementary condition (SSC). Choosing an SSC is associated with fixing a reference frame the motion is observed in. The choice of the SSC depends on the question one wants to investigate [13–21]. We use the Tulczyjew condition (T SSC) [21] which corresponds to the zero 3-momentum frame. The dynamics of spinning test-particles has been worked out in Lagrangian and Hamiltonian formalisms of which the latter appears to be more complicated [22–

*Electronic address: daniela.kunst@zarm.uni-bremen.de

†Electronic address: volker.perlick@zarm.uni-bremen.de

‡Electronic address: claus.laemmerzahl@zarm.uni-bremen.de

24]. For the motion of spinning test-particles in the Schwarzschild or Kerr spacetime we refer, e.g., to [25–27] and for the case that also the quadrupole moment of the test-particle is taken into account to [28]. Several papers have been devoted to the question of whether the motion is chaotic, which also has a great impact on the analysis of possible gravitational wave signals [29–32].

The paper is organized as follows. In the second section we recall the equations of motion for non-spinning and spinning test-particles in Schwarzschild-de Sitter spacetime. In particular we specify the region of bound motion. After that we analyze the frequencies of bound motion and find the domain where isofrequent orbits exist in section three. Lastly, we summarize our results and give an outlook for future work and applications.

2. MOTION IN SCHWARZSCHILD DE SITTER SPACETIME

2.1. Non-spinning particles

Schwarzschild-de Sitter spacetime is the unique spherically symmetric vacuum solution to Einstein’s field equations including a positive cosmological constant, $\Lambda > 0$, see e.g. Rindler [33]. For a negative cosmological constant it is called Schwarzschild-anti-de Sitter spacetime, but here we are interested only in the case $\Lambda > 0$. The metric reads [33]

$$ds^2 = -f(r) dt^2 + f(r)^{-1} dr^2 + r^2 (d\theta^2 + \sin^2(\theta) d\phi^2) \quad (1)$$

in spherical coordinates with

$$f(r) = 1 - \frac{2M}{r} - \frac{\Lambda}{3} r^2. \quad (2)$$

Here M corresponds to the mass of the gravitating body and the units are chosen such that $c = 1$ and $G = 1$. We consider only the region $r > 0$. For $0 < \Lambda < (3M)^{-2}$, the function $f(r)$ has two zeros, indicating two horizons, at radii r_{H1} and r_{H2} with $2M < r_{H1} < 3M < r_{H2}$; the metric is static in the region $r_{H1} < r < r_{H2}$ where $f(r) > 0$. For $\Lambda > (3M)^{-2}$ there is no horizon and no static region.

The dynamics of massive non-spinning test-particles is determined by the geodesic equation for timelike curves. Since the spacetime is spherically symmetric the motion takes place in a plane, which we choose to be the equatorial plane $\theta = \frac{\pi}{2}$. Then the equations of motion, parametrized by proper time τ , for a test-particle of mass m read

$$m^2 \left(\frac{dt}{d\tau} \right)^2 = \frac{H^2}{f(r)^2}, \quad (3)$$

$$m^2 \left(\frac{dr}{d\tau} \right)^2 = H^2 - f(r) \left(\frac{J_z^2}{r^2} + m^2 \right), \quad (4)$$

$$m^2 \left(\frac{d\phi}{d\tau} \right)^2 = \frac{J_z^2}{r^4}, \quad (5)$$

with H and J_z being two constants of motion to be interpreted as the energy and the angular momentum, respectively. The particle’s four-momentum is $p^\mu = m \frac{dx^\mu}{d\tau}$ and satisfies the mass-shell condition $m^2 = -p_\mu p^\mu$. From hereon we rescale $H \mapsto Hm$ and $J_z \mapsto J_z m$ which is tantamount to setting $m = 1$ in (3), (4) and (5). Then H is dimensionless while J_z has the dimension of a length.

In the following we are interested only in bound motion, i.e., in orbits that have two turning points, an apastron r_a and a periastron r_p , where $dr/d\tau = 0$. From (4) it is obvious that turning points can exist only at radial coordinates where $f(r) > 0$. This implies that bound orbits are confined to the region between the two horizons. In particular they do not exist if $\Lambda > (3M)^{-2}$.

We rewrite (4) as

$$\left(\frac{dr}{d\tau} \right)^2 = \frac{\Lambda}{3r^3} P_5(r), \quad (6)$$

where

$$P_5(r) = r^5 - \left((1 - H^2) \frac{3}{\Lambda} - J_z^2 \right) r^3 + \frac{6M}{\Lambda} r^2 - \frac{3}{\Lambda} J_z^2 r + \frac{6M}{\Lambda} J_z^2. \quad (7)$$

As we assume $\Lambda > 0$, the region where $P_5(r) < 0$ is forbidden by (6). The number of zeros of $P_5(r)$ determines the types of motion possible for the corresponding values of H and J_z . For positive Λ there can be at most four positive real zeros as can be derived with the rule of signs by Descartes. Bound orbits are allowed only when the polynomial has precisely four positive zeros. For other values of H and J_z there will be escape or terminating orbits or no motion at all.

From now on we rescale $r \mapsto rM$, $J_z \mapsto J_z M$ and $\Lambda \mapsto \Lambda M^{-2}$ so that these quantities are dimensionless. (Recall that H already was dimensionless.) This is tantamount to setting $M = 1$ in (7). Since we must have four positive real zeros in order to consider bound motion we can rewrite equation (7) as

$$P_5(r) = (r - r_0)(r - r_1)(r - r_p)(r - r_a)(r - r_2) \quad (8)$$

with $r_0 < 0 < r_1 < r_p < r_a < r_2$. Bound motion exists only between r_p and r_a . Also, the motion is fully described by the parameters r_a and r_p , because H and J_z can be expressed in terms of r_a and r_p ,

$$H^2 = \frac{\left(\frac{\Lambda}{3} r_a^3 - r_a + 3 \right) \left(\frac{\Lambda}{3} r_p^3 - r_p + 3 \right) (r_a + r_p)}{r_a^2 (r_p - 2) + r_p^2 (r_a - 2) - 2r_a r_p}, \quad (9)$$

$$J_z^2 = \frac{r_a^2 r_p^2 (3 - \frac{\Lambda}{3} r_a r_p (r_a + r_p))}{r_a^2 (r_p - 2) + r_p^2 (r_a - 2) - 2r_a r_p}. \quad (10)$$

Therewith we can find all the zeros of (7) expressed in terms of r_p and r_a . Comparing the coefficients of the two equations (7) and (8) yields expressions for r_0 and r_2 dependent on (r_1, r_a, r_p) and the equation

$$P_3(r_1) := \Lambda r_a^2 r_p^2 r_1^3 + \Lambda r_a^2 r_p^2 (r_a + r_p) r_1^2 + J_z^2 (6r_p - 3r_a(r_p - 2)) r_1 + 6J_z^2 r_a r_p \stackrel{!}{=} 0 \quad (11)$$

so that we only have to solve a cubic equation for r_1 .

In the (H, J_z) -plane, the boundaries of bound motion are determined by the merging of two zeros or by the condition that the orbit becomes unbound. Physically, a merging $r_a = r_p$ corresponds to a stable circular orbit. A merging $r_1 = r_p \neq r_a = r_2$ corresponds to an unstable circular orbit at r_p and a homoclinic orbit from r_p to r_a and back to r_p , while a merging $r_1 \neq r_p \neq r_a = r_2$ corresponds to an unstable circular orbit at r_a and a homoclinic orbit from r_a to r_p and back to r_a . In the case that $r_1 = r_p \neq r_a = r_2$ we have unstable circular orbits at r_p and at r_a and heteroclinic orbits from r_a to r_p and from r_p to r_a .

Another parametrization of bound orbits is given by the semi-latus rectum p and the eccentricity e . The relations to the periastron r_p and the apastron r_a are

$$r_a = \frac{p}{1-e}, \quad r_p = \frac{p}{1+e}. \quad (12)$$

We choose this parametrization since then the analysis of the properties of a test particle's motion is more convenient.

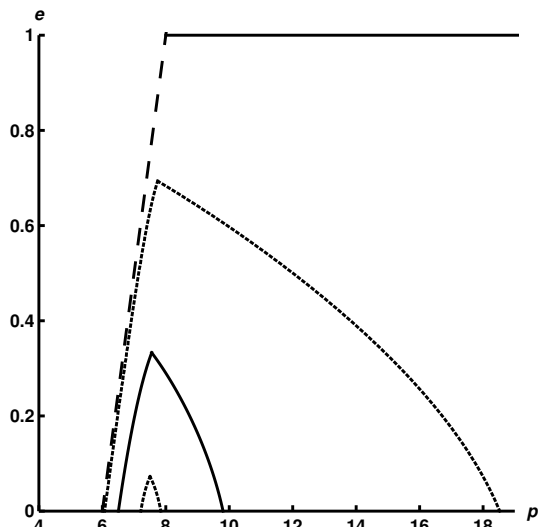


Figure 1: The figure presents the regions of bound motion in the (p, e) -plane for different values of Λ . The dashed line is the separatrix in the Schwarzschild case, $\Lambda = 0$, given by the equation $p = 6 + 2e$. The remaining lines are the separatrices for a cosmological constant of $\Lambda = 0.0001$ (upper dotted line), $\Lambda = 0.0005$ (solid line), and $\Lambda = 0.0006$ (lower dotted line).

In Fig. 1 the region of bound motion is shown in a (p, e) -diagram for both Schwarzschild and Schwarzschild-de Sitter spacetimes. We first consider the Schwarzschild case for which the general features of the domain of bound orbits have been discussed already by Cutler, Kennefick and Poisson [34], see also [44] and [1, 2]. In this case the domain of bound orbits, corresponding to the region that lies to the right of the dashed line, is infinitely large. This dashed line, which is given by the equation

$p = 6 + 2e$, is often called the *separatrix* because it separates the region of bound orbits from the region of unbound orbits. On the separatrix, each point corresponds to a homoclinic orbit from a radius $r_1 = r_p$ to a radius $r_a > r_p$ and back to $r_1 = r_p$. Such a homoclinic orbit has the same constants of motion H and J_z as the unstable circular orbit at $r_1 = r_p$ which it asymptotically approaches. Bound orbits near the separatrix are periodically “zooming out” to the apastron with many “whirls” near the periastron in between, see Levin, O’Reilly and Copeland [45]; such *zoom-whirl* orbits have also been discussed in [42–44]. The upper boundary curve of the region of bound orbits corresponds to unbound (parabolic-type) orbits with $e = 1$, while the lower boundary corresponds to stable circular orbits with $e = 0$. The lower left-hand corner of the region of bound orbits corresponds to the innermost stable circular orbit (ISCO) at $r = 6$.

By contrast, in the Schwarzschild-de Sitter spacetime the region of bound orbits in the (p, e) -plane is finite. The shape is triangle-like with its tip at an eccentricity $e_{\max} < 1$. This demonstrates that, in this picture, the transition from bound orbits to unbound orbits ($e > 1$) is not continuous. In analogy to the Schwarzschild case, the two sides of the triangle are called the *separatrices*. They correspond to homoclinic orbits with $r_1 = r_p$ and $r_a = r_2$, respectively. Each homoclinic orbit has the same values for energy and angular momentum as the unstable circular orbit that it approaches asymptotically. We have already mentioned that in the Schwarzschild spacetime bound orbits near the separatrix show a zoom-whirl behavior, with the “whirling” taking place in the strong-field regime. In the Schwarzschild-de Sitter spacetime with a small positive cosmological constant, the second separatrix gives rise to zoom-whirl orbits that “whirl” near an apastron far away from the center and periodically “zoom in” to a periastron. The two separatrices intersect at the tip of the triangle where we have simultaneously $r_1 = r_p$ and $r_a = r_2$. This gives rise to a heteroclinic orbit, i.e., to an orbit that connects two different unstable circular orbits. Such an orbit can be described by a unique pair of values for (p, e) . The lower boundary curve of the region of bound orbits corresponds to stable circular orbits. The two intersection points of the separatrices with the horizontal axis correspond to the innermost stable circular orbit (ISCO) and the outermost stable circular orbit (OSCO). While the ISCO is also present in the Schwarzschild spacetime and merely gets shifted away from the center with increasing Λ , the OSCO is only existent in the Schwarzschild-de Sitter spacetime. For $\Lambda \rightarrow 0$ the OSCO approaches infinity. For $\Lambda \rightarrow \Lambda_{\text{crit}} = 4/5625$ the ISCO and the OSCO merge into one circular orbit, cf. [7]. Put into mathematical language, this happens if all four positive zeros of (7) coincide. For $\Lambda > \Lambda_{\text{crit}}$ bound orbits do not exist. Let us remark here that Λ_{crit} is much larger than the physically expected value of the cosmological constant. Observations show evidence for a $\Lambda \approx 10^{-52} \text{m}^{-2}$ [36]. Even for a supermassive black hole with $M \approx 10^{10} \text{km}$ this corre-

sponds, in our geometrized units, to $\Lambda \approx 10^{-25}$, i.e., to a value that is much smaller than Λ_{crit} .

2.2. Spinning particles in the equatorial plane

Now we turn on the spin and investigate the motion of a spinning test-particle which is no longer geodesic. The corresponding equations of motion are the well-known Mathisson-Papapetrou-Dixon equations [10–12],

$$\dot{p}^\mu = -\frac{1}{2}R^\mu_{\nu\kappa\lambda}u^\nu S^{\kappa\lambda}, \quad (13)$$

$$\dot{S}^{\mu\nu} = pu^\nu - p^\nu u^\mu. \quad (14)$$

Here $R^\mu_{\nu\kappa\lambda}$ is the curvature tensor of the underlying spacetime, the dot denotes differentiation with respect to proper time τ along the worldline of the particle, p^μ is the four-momentum and u^μ is the four-velocity of the particle, and $S^{\mu\nu}$ is the antisymmetric spin tensor. As already mentioned in the introduction, the set (13)-(14) is underdetermined; a so-called *supplementary spin condition* (SSC) must be chosen in order to get a well-posed initial-value problem. In this work the Tulczyjew condition [21] is chosen,

$$S^{\mu\nu}p_\nu = 0. \quad (15)$$

Then the relation between p_μ and u^ν can be given explicitly: Using the conserved quantity $m^2 = -p_\mu p^\mu$, introducing the normalized momentum vector $\hat{p}^\mu = \frac{p^\mu}{m}$ and renormalizing the four-velocity such that $\hat{p}^\mu \hat{u}_\mu = -1$ allows to derive the relation [37]

$$\hat{u}^\mu - \hat{p}^\mu = \frac{S^{\mu\nu}R_{\nu\gamma\sigma\lambda}\hat{p}^\gamma S^{\sigma\lambda}}{2(m^2 + \frac{1}{4}R_{\alpha\beta\delta\xi}S^{\alpha\beta}S^{\delta\xi})}. \quad (16)$$

Therewith, it is now possible to derive the equations of motion for a spinning test-particle in Schwarzschild-de Sitter spacetime. However, here we will restrict ourselves to the special case of a particle moving in the equatorial plane, with the spin vector perpendicular to this plane. Then we can characterize the spin by the scalar constant of motion S , defined by

$$S^2 = S^\mu S_\mu, \quad S^\mu = \frac{1}{2}\varepsilon^{\mu\nu\sigma\tau}\hat{p}_\nu S_{\sigma\tau} \quad (17)$$

with the totally antisymmetric Levi-Civita tensor field, and the property that S is positive if the spin is parallel to the orbital angular momentum and negative if it is anti-parallel. As in the spinless case, we have a conserved energy H and a conserved angular momentum J_z which we rescale according to $H \mapsto Hm$ and $J_z \mapsto J_z m$. In addition, we now also rescale the spin, $S \mapsto sm$. The resulting equations of motion can be taken from [37], after

appropriate adaptation,

$$\left(\frac{dt}{d\tau}\right) = \frac{H + \frac{f'(r)}{2r}sJ_z}{\Pi_s(r)\Sigma_s(r)f(r)}, \quad (18)$$

$$\left(\frac{dr}{d\tau}\right) = \pm \frac{\sqrt{R_s(r)}}{\Pi_s(r)\Sigma_s(r)}, \quad (19)$$

$$\left(\frac{d\phi}{d\tau}\right) = \frac{(J_z - Hs)\left(1 - \frac{f''(r)}{2}s^2\right)}{\Pi_s(r)\Sigma_s(r)^2 r^2}. \quad (20)$$

Here $f(r)$ is defined by (2), the prime denotes derivative with respect to r , and

$$\Pi_s(r) = 1 + \frac{\left(f''(r) - \frac{f'(r)}{r}\right)(J_z - Hs)^2 s^2}{2r^2 \Sigma_s(r)^3}, \quad (21)$$

$$\Sigma_s(r) = 1 - \frac{f'(r)}{2r}s^2, \quad (22)$$

$$R_s(r) = \left(H - \frac{f'(r)}{2r}sJ_z\right)^2 - f(r)\left\{\Sigma_s(r)^2 + \frac{(J_z - Hs)^2}{r^2}\right\}. \quad (23)$$

Again we are interested in bound motion, so we require two turning points r_a and r_p where $dr/d\tau = 0$ which corresponds to $R_s(r) = 0$. We rescale, as before, $r \mapsto rM$, $J_z \mapsto J_z M$, $\Lambda \mapsto \Lambda M^{-2}$ and now also $s \mapsto sM$. Note that for test particle motion our dimensionless spin parameter s necessarily satisfies the condition $-1 < s < 1$, see [30]. Moreover, we substitute

$$L = J_z - Hs \quad (24)$$

for mathematical convenience. Then $R_s(r)$ can be rewritten as

$$R_s(r) = \frac{\Lambda\left(1 + \frac{\Lambda}{3}s^2\right)^2}{3r^7}P_9(r) \quad (25)$$

where

$$P_9(r) = r^9 + ar^7 + br^6 + cr^5 + dr^4 + er^3 + gr + h \quad (26)$$

with

$$a = \frac{\left(H \left(1 + \frac{\Lambda}{3}s^2\right) + \frac{\Lambda}{3}Ls\right)^2 + \frac{\Lambda}{3}L^2}{\frac{\Lambda}{3} \left(1 + \frac{\Lambda}{3}s^2\right)^2} - \frac{3}{\Lambda}, \quad (27)$$

$$b = \frac{2}{\frac{\Lambda}{3} \left(1 + \frac{\Lambda}{3}s^2\right)}, \quad (28)$$

$$c = -\frac{L^2}{\frac{\Lambda}{3} \left(1 + \frac{\Lambda}{3}s^2\right)^2}, \quad (29)$$

$$d = -\frac{2 \left((L + Hs)^2 - s^2\right)}{\frac{\Lambda}{3} \left(1 + \frac{\Lambda}{3}s^2\right)} + \frac{2L(2L + Hs)}{\frac{\Lambda}{3} \left(1 + \frac{\Lambda}{3}s^2\right)^2}, \quad (30)$$

$$e = -\frac{4s^2 \left(1 + \frac{\Lambda}{3}s^2\right)}{\frac{\Lambda}{3} \left(1 + \frac{\Lambda}{3}s^2\right)^2}, \quad (31)$$

$$g = \frac{s^2 \left((L + Hs)^2 - s^2\right)}{\frac{\Lambda}{3} \left(1 + \frac{\Lambda}{3}s^2\right)^2}, \quad (32)$$

$$h = \frac{2s^4}{\frac{\Lambda}{3} \left(1 + \frac{\Lambda}{3}s^2\right)^2}. \quad (33)$$

The number of zeros of $P_9(r)$ determines the types of motion possible in the corresponding spacetime. Finding the maximum number of positive real zeros in this case is not so easy, though, since the signs of a and d are unclear. (The sign of g does not matter because the signs of e and h are already different.) In any case, from Descartes' rule of signs we find that the number of positive real zeros can only be 0, 2, 4 or 6. Again, in order to consider bound motion we must have at least four positive real zeros. We argue that in this case (26) can be written as

$$P_9(r) = (r - r_\gamma)(r - r_\beta)(r - r_\alpha)(r - r_1) \times (r - r_p)(r - r_a)(r - r_2)(r - r_I)(r - \bar{r}_I) \quad (34)$$

with $r_\gamma < r_\beta < r_\alpha < 0 < r_1 < r_p < r_a < r_2$ and r_I, \bar{r}_I being some non-real complex zero and its conjugate, respectively. The knowledge of a non-real zero was obtained by checking the signs of the coefficients in the relevant parameter space. To exclude the case with six positive real zeros, we observe that in the relevant range of parameters, $0 < \Lambda < 1/9$ and $-1 < s < 1$, only three mergers of zeros exist. Therefore we conclude to have one pair of complex zeroes.

Bound motion exists only between r_p and r_a . Since also for the spinning particle the motion is fully described by the parameters r_a and r_p , we find expressions for $H(r_a, r_p)$ and $L(r_a, r_p)$ by setting $R_s(r_a) = 0$ and $R_s(r_p) = 0$. With the help of (12) the expressions are converted to $H(p, e)$ and $L(p, e)$. The next task is to find the boundaries of the region of bound motion in the (p, e) -plane, i.e. the separatrices. Again, the boundaries are given by the merging of two zeros, $r_1 = r_p$ or/and $r_p = r_a$ or/and $r_a = r_2$. Unfortunately, the explicit expressions for the zeros are not as easily found as in the non-spinning case. However, there is a way around: We

simply exploit the fact that the values of H and L for the homoclinic orbits are identical to the ones for the unstable circular orbits which they approach asymptotically. Having access to the values of H and L for circular orbits by solving $R_s(r) = 0$ and $R'_s(r) = 0$, the only computation needed is to find the intersection point of the lines of constant H and constant L in the (p, e) -plane. In this way we obtain the values for p and e of the homoclinic orbits corresponding to the separatrices.

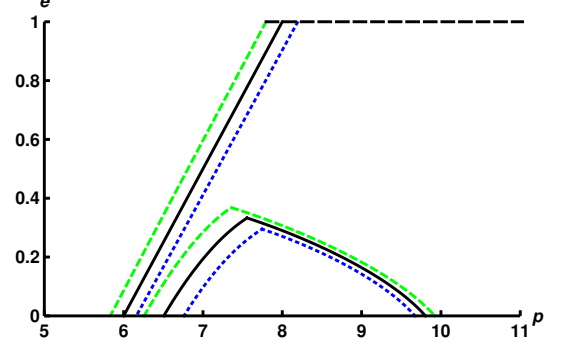


Figure 2: The figure presents the regions of bound motion in the (p, e) -plane for different values of s for $\Lambda = 0$ as well as $\Lambda = 0.0005$. The straight lines on the left correspond to $\Lambda = 0$ and the triangles on the right correspond to $\Lambda = 0.0005$. In either case, the (green) dashed line corresponds to $s = 0.1$, the black solid line to $s = 0$, and the (blue) dotted line to $s = -0.1$.

In Fig. 2 the region of bound motion is shown in a (p, e) -diagram for both a spinning and a non-spinning particle moving in Schwarzschild and Schwarzschild-de-Sitter spacetime. Here, we have fixed the cosmological constant either to $\Lambda = 0$ or to $\Lambda = 0.0005$ and varied the value of the spin parameter.

From Fig. 2 we read that for a spinning particle in Schwarzschild spacetime the region of bound motion is infinitely large as it is for geodesic motion. The well-known shift of the ISCO due to the spin is visible, such that for positive spin it is moved inwards and for negative spin outwards, cf. [39] and also [38, 40]. This reflects the coupling of the particle's spin to its orbital angular momentum. If they are parallel to each other the resulting force is repulsive, while it is attractive if they are antiparallel [39]. Notice that the upper boundary is given by $e = 1$ which corresponds to parabolic orbits and marks the transition from bound motion to unbound orbits. By and large, the general shape of the separatrices resembles the one for non-spinning particles in Schwarzschild spacetime.

When a positive cosmological constant is considered, the value of the maximal eccentricity becomes smaller for negative and larger for positive spin. Correspondingly, the critical value of Λ is also shifted: for positive spin Λ_{crit} is bigger than for the spinless case and for negative spin it is smaller. The dependence of Λ_{crit} on the spin is shown in Fig. 3.

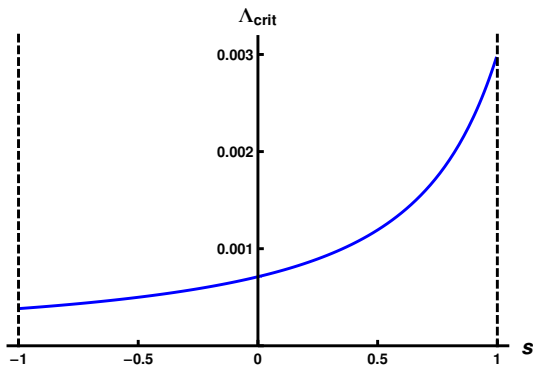


Figure 3: The figure presents the dependence of the critical value of Λ on the spin parameter. It monotonically increases with the spin. The boundaries $s = -1$ and $s = 1$ are due to physical restrictions.

It reveals that for $\Lambda < \Lambda_{crit}(s = 0) = 4/5625$ bound motion is possible for all positive spin values but not for all negative spin values. This is the reason why for our particular choice of $\Lambda = 0.0005$ it is not possible to have bound orbits with spins that are smaller than ≈ -0.5 . As soon as the chosen value of Λ drops below $\Lambda_{crit}(s = -1) \approx 0.0004$ bound motion is possible for all spin values $-1 < s < 1$.

The influence of the spin on the ISCO in the Schwarzschild-de Sitter spacetime is similar as in the Schwarzschild spacetime. Again we see that for positive spin parameters the ISCO gets shifted towards the center and for negative spin parameters away from the center. For the OSCO it is the other way around. By taking into account these two characteristics as well as the shift of the maximal eccentricity, it can be immediately seen that the region of bound orbits becomes smaller for negative spin and gets larger for positive spin.

One might think that a large positive spin is somehow able to destroy the existence of the heteroclinic orbit sitting at maximal eccentricity. However, even if the spin is chosen to have its maximal value of 1 the shape of the region of bound motion does not change. The triangle survives and with it the heteroclinic orbit. If Λ approaches zero the maximal eccentricity goes to 1 and the OSCO to infinity, for any spin value. In this case the separatrix resembles the one of Schwarzschild, only shifted closer to the center for $s > 0$ and farther away from the center for $s < 0$.

In the following section we change from the parametrization of bound orbits in terms of p and e to the frequency domain. This will allow us to discuss the phenomenon of isofrequency pairing.

3. ISOFREQUENCY PAIRING

As mentioned before, Barack and Sago [1] observed that for bound orbits of spinless test-particles in the

Schwarzschild spacetime the transformation from the constants of motion H and J_z to the radial and azimuthal frequencies becomes degenerate in the highly relativistic regime. In particular, it was demonstrated that orbits exist with different eccentricities but with the same frequency pair.

Here, we show how the picture of this degeneracy phenomenon changes if a cosmological constant is turned on and if the particle's spin is incorporated. Generally, the frequencies are defined as [34]

$$\Omega_r = \frac{2\pi}{T_r}, \quad \Omega_\phi = \frac{\Delta\phi}{T_r} \quad (35)$$

with

$$T_r = 2 \int_{r_p}^{r_a} \frac{dt}{dr} dr = 2 \int_{r_p}^{r_a} \frac{dt}{d\tau} \left(\frac{dr}{d\tau} \right)^{-1} dr, \quad (36)$$

$$\Delta\phi = 2 \int_{r_p}^{r_a} \frac{d\phi}{d\tau} \left(\frac{dr}{d\tau} \right)^{-1} dr. \quad (37)$$

In correspondence with our choice of units in the previous sections we rescale $\Omega_r \rightarrow \Omega_r/M$ and analogously $\Omega_\phi \rightarrow \Omega_\phi/M$.

3.1. Non-spinning particles

Again, we start with the geodesic motion. From equations (3)-(8) we obtain

$$T_r = 2H \sqrt{\frac{3}{\Lambda}} \int_{r_p}^{r_a} \frac{r^2 dr}{f(r) \sqrt{r P_5(r)}}, \quad (38)$$

$$\Delta\phi = 2L \sqrt{\frac{3}{\Lambda}} \int_{r_p}^{r_a} \frac{dr}{\sqrt{r P_5(r)}}, \quad (39)$$

with $f(r)$ from (2) and $P_5(r)$ from (7). As the polynomial $r P_5(r)$ under the root in the denominator of the integrand is of order 6, the integral is of hyperelliptic type, which cannot be integrated in terms of elementary functions.

If we use, as before, the (p, e) parametrization of the bound orbits, we may substitute the integration variable r in (38) and (39) according to

$$r = \frac{p}{1 + e \cos \chi} \quad (40)$$

where the new integration variable χ is the relativistic anomaly. Then the boundary values of the integral change to 0 and π .

Since we want to compare the frequencies of different orbits, we choose in analogy to Warburton et al. [2] the (Ω_ϕ, e) parametrization for our analysis of bound orbits, which we are allowed to because Ω_ϕ monotonically decreases with p if the eccentricity is held fixed. In order to do this we have to deal with several obstacles. First, we cannot analytically invert the Ω_ϕ integral to obtain p as

a function of e and Ω_ϕ . To circumvent this hindrance the value for e is fixed in the integral for the frequency, so that the value for p can be computed using a root-finding method for any allowed Ω_ϕ . In this way we obtain the value for p for any given e and Ω_ϕ ; that is to say, we numerically acquire a function $p(e, \Omega_\phi)$. Hence, the radial frequency can also be written as a function $\Omega_r(e, \Omega_\phi)$ and we are able to plot contour lines for constant Ω_r into an (Ω_ϕ, e) -diagram.

Secondly, we encounter problems close to the separatrices. Both T_r and $\Delta\phi$ diverge at the separatrices making it numerically challenging to perform the computations for the frequencies. Luckily, there exists an approximation scheme for hyperelliptic integrals developed by Sochnev [35] based on the approximation of irrational numbers. We rewrite the integrals of (38) and (39) with the substitution

$$r = \frac{(r_a + r_p) + (r_a - r_p)x}{2} \quad (41)$$

to obtain

$$T_r = A(r_p, r_a, \Lambda) \int_{-1}^1 \frac{V_t(x) dx}{\sqrt{V_r(x)}}, \quad (42)$$

$$\Delta\phi = B(r_p, r_a, \Lambda) \int_{-1}^1 \frac{dx}{\sqrt{V_r(x)}}, \quad (43)$$

where $V_t(x)$ is a rational function whose denominator has no zeros in the integration interval and

$$V_r(x) = (1-x^2)(1+k_1x)(1+k_2x)(1+k_3x)(1+k_4x) \quad (44)$$

with

$$\begin{aligned} k_1 &= \frac{r_a - r_p}{r_a + r_p}, \\ k_2 &= \frac{r_a - r_p}{(r_a - r_0) + (r_p - r_0)}, \\ k_3 &= \frac{r_a - r_p}{(r_a - r_1) + (r_p - r_1)}, \\ k_4 &= -\frac{r_a - r_p}{(r_2 - r_a) + (r_2 - r_p)}, \end{aligned}$$

which satisfy $0 \leq k_2 \leq k_1 \leq k_3 \leq 1$ and $-1 \leq k_4 \leq 0$. If we get close to the separatrices either k_3 or $-k_4$ approaches 1. For each of these two cases Sochnev's method allows to approximate the integrals (42) and (43) in terms of elementary integrals, see the Appendix. Consequently, the frequencies close to the separatrix can be approximately expressed in terms of elementary functions. Now we have the tools we need for analyzing the behavior of the frequencies in the region of bound motion.

In Fig. 4 the region of bound orbits is shown in the (Ω_ϕ, e) -plane. It is the shape of this region that is striking. It looks no longer like a triangle, as in the (p, e) -representation, but more like a trapezoid. The tip of the triangle is stretched out to a straight line at e_{\max} . In the (p, e) -representation the heteroclinic orbit corresponds to

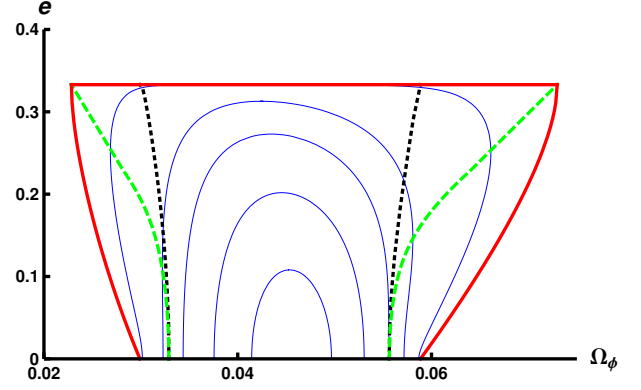


Figure 4: The figure depicts the phenomenon of isofrequency pairing for bound orbits in the (Ω_ϕ, e) -plane for a fixed $\Lambda = 0.0005$. The thick (red) boundary lines correspond to the separatrices and confine the region of bound motion. The (blue) solid lines inside this region correspond to constant values of Ω_r . The (green) dashed lines are the singular curves, i.e. the locus where the Jacobian determinant of the transformation from (p, e) to (Ω_r, Ω_ϕ) vanishes. Isofrequency pairing occurs in two domains each of which is bounded by a separatrix and a curve of Circular Orbit Duals (COD). The COD curves are shown by the dotted black lines.

a single point – the tip of the triangle – since it has a uniquely defined pair (r_p, r_a) . By contrast, the azimuthal frequency is not uniquely defined for the heteroclinic orbit. Note that the original definition of the frequencies is valid only within the region of bound orbits. On the boundaries, that is at the separatrices, the frequencies are defined only by a continuous extension which assigns unique frequencies to the homoclinic orbits. However, in the case of the heteroclinic orbit the value of Ω_ϕ depends on how the orbit is approached. This is the reason why the heteroclinic orbit is stretched out to a straight line in the (Ω_ϕ, e) -diagram. A bound orbit that lies close to this line could be called a “whirl-whirl orbit” because it periodically changes between a large number of whirls near its apastron and a large number of whirls near its periastron.

The main property we are interested in is the isofrequency pairing. This phenomenon is easily seen in the diagram close to the two separatrices. Looking at a contour line for $\Omega_r = \text{constant}$ near one of the separatrices, we see that it has two intersection points with a contour line for $\Omega_\phi = \text{constant}$, i.e., with a vertical line in this diagram. Since these intersection points correspond to orbits of different eccentricities, we conclude that there exist two geometrically distinct orbits with the same pair of frequencies. In mathematical terms this means that the transformation from the frequencies (Ω_r, Ω_ϕ) to (p, e) is not one-to-one. In order to prove this degeneracy it is sufficient to show that the Jacobi determinant

$$J = \left| \frac{\partial(\Omega_r, \Omega_\phi)}{\partial(p, e)} \right| \quad (45)$$

becomes singular somewhere within the region of bound orbits. In Fig. 4 these singular points can be found as the points where the tangents to the contour lines of $\Omega_r = \text{constant}$ become vertical. This happens along the

two (green) dashed curves in Fig. 4 which are called the *singular curves*. To verify that J does have two zeros close to $e = 0$, one may perform a Taylor expansion of J about $e = 0$ up to first order,

$$J = \frac{eP_{10}(p)}{4p^4 \sqrt{p(\frac{\Lambda}{3}p^3 - 1)(\frac{\Lambda}{3}p^3 - p + 2)(\frac{\Lambda}{3}(4p - 15)p^3 - p + 9)^{3/2}}} + O(e^2)$$

with

$$P_{10}(p) = 15\Lambda^3 p^{10} - 50\Lambda^3 p^9 + 30\Lambda^2 p^8 - 315\Lambda^2 p^7 + 9\Lambda(80\Lambda - 1)p^6 - 45\Lambda p^5 + 918\Lambda p^4 - 2241\Lambda p^3 + 108p^2 - 1053p + 2322.$$

Numerically one finds that the tenth order polynomial $P_{10}(p)$ has precisely two positive real zeros lying within the allowed range of p values for bound motion, for all $0 < \Lambda < 1/9$.

The isofrequency pairs lie on opposite sides of one of the singular curves, i.e., each orbit that is located between a separatrix and a singular curve has a partner orbit on the other side of the corresponding singular curve which is geometrically different but has the same pair of frequencies. The regions where isofrequency pairing occurs are bounded by the so-called ‘‘Circular Orbit Dual’’ (COD) curves which are represented by the black dashed lines. A point on a COD curve corresponds to an orbit that has the same frequencies as a stable circular orbit situated between one of the singular curves and the corresponding separatrix.

In comparison to the Schwarzschild spacetime, the most interesting new feature of isofrequency pairing in the Schwarzschild-de Sitter spacetime is in the fact that this phenomenon now occurs not only in the highly relativistic regime close to the center but also in a region far away from the center.

While we could read from Fig. 1 how the ISCO radius, the OSCO radius and the maximal eccentricity depend on Λ , Fig. 4 gives us information on the frequencies of bound motion. A quite interesting property is the existence of a maximal radial frequency. From Fig. 4 we read that the lines of constant Ω_r have the shape of semicircles which become smaller in the center of the diagram. The value of Ω_r varies between $\Omega_r = 0$ on the separatrices and a maximal value when the semicircle is contracted to just one single point. Fig. 5 shows a parametric plot of the maximal value of Ω_r against p , where the parameter is the cosmological constant. As Ω_r takes its maximal value on the axis $e = 0$, i.e., for the limiting case of a circular orbit, p is the same as the radius coordinate. We see that the position where Ω_r takes its maximal value varies between $p = 8$ for $\Lambda = 0$ and $p = 7.5$ for $\Lambda = \Lambda_{\text{crit}} = 4/5625$.

Moreover, we can read from Fig. 5 that the presence of a positive cosmological constant introduces another kind of degeneracy. Notice that Ω_r^{max} decreases slightly when

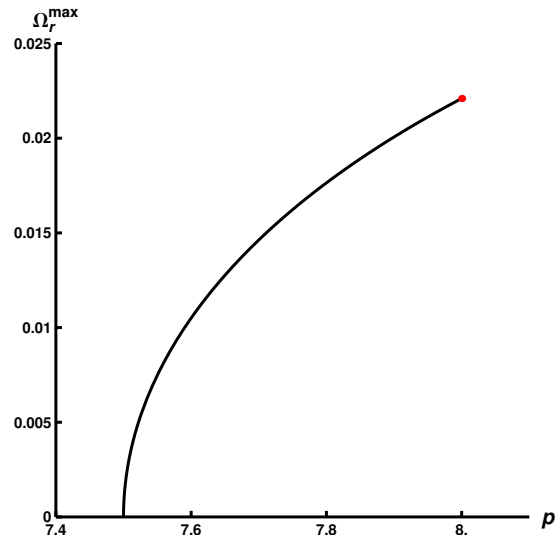


Figure 5: The figure shows how the value of Ω_r^{max} and the position where this value is taken depend on Λ . The (red) dot marks the Schwarzschild case with $\Lambda = 0$. Along the solid black line Λ increases up to its maximal value of $1/9$ where the bound orbits vanish.

Λ is slightly increased. Transferring this change to Fig. 4 we can think of the lines of constant Ω_r getting shifted towards the center. Imagine that we have a frequency pair close to the right separatrix. Choose the outer contour line of $\Omega_r = \text{constant}$ and let some vertical line of constant Ω_ϕ intersect it twice and mark these two points. As described above, they are two orbits with the same frequencies. If the cosmological constant is changed a little bit the line of constant Ω_r gets shifted either to the right if Λ is reduced or to the left if Λ is amplified. However, we would still have two intersection points with the vertical line representing the azimuthal frequency we have fixed before. If Λ is reduced the two intersection points diverge while for amplified Λ the intersection points approach one another, i.e. their eccentricities change. This means that infinitely many physically distinct pairs of

orbits have the same frequencies as the originally fixed one if we allow the cosmological constant to take values in a certain interval.

In the next section we discuss what happens to the degeneracy features when a spin of the particle is added.

3.2. Spinning particles in the equatorial plane

As before, we are interested in the influence of a particle's spin on its motion and dynamical properties. From (18)-(20) we obtain

$$T_r = 2\sqrt{\frac{3}{\Lambda}} \int_{r_p}^{r_a} \frac{\tilde{V}_t^s(r)}{\sqrt{rP_9(r)}} dr, \quad (46)$$

$$\Delta\phi = 2L\sqrt{\frac{3}{\Lambda}} \int_{r_p}^{r_a} \frac{\tilde{V}_\phi^s(r)}{\sqrt{rP_9(r)}} dr, \quad (47)$$

$$(48)$$

with $P_9(r)$ from (26) and

$$\tilde{V}_t^s(r) = \frac{r^2 \left[H \left(r^3 + \left(\frac{\Lambda}{3} r^3 - 1 \right) s^2 \right) + \left(\frac{\Lambda}{3} r^3 - 1 \right) sL \right]}{\left(-\frac{\Lambda}{3} r^3 + r - 2 \right) \left(1 + \frac{\Lambda}{3} s^2 \right)}, \quad (49)$$

$$\tilde{V}_\phi^s(r) = \frac{r^2 \left(r^3 + \left(\frac{\Lambda}{3} r^3 + 2 \right) s^2 \right)}{\left(r^3 + \left(\frac{\Lambda}{3} r^3 - 1 \right) s^2 \right) \left(1 + \frac{\Lambda}{3} s^2 \right)}. \quad (50)$$

The order of the polynomial $rP_9(r)$ under the root in the denominator of the integrand is 10. Therefore we now have a considerably more difficult kind of hyperelliptic integral than in the spinless case.

Following the same procedure as in the non-spinning case, we transform the integrals with $r = \frac{p}{1+e\cos\chi}$ to obtain the resulting frequencies as functions of (p, e) . Therewith, we are able to reparametrize the radial frequency, again, as a function of (Ω_ϕ, e) so that the comparison of different orbits and their frequencies is simplified. Since the inclusion of the spin does not make the system easier to be solved, we encounter the same numerical problems as before, i.e. the numerical inversion to $p(\Omega_\phi, e)$ and the divergencies close to the separatrices, as we have in the non-spinning case. Luckily, these problems can be tackled also by the same method, only the expressions become more complicated.

Employing Sochnev's approach of approximating hyperelliptic integrals we rewrite the integrals of (46) and (47) with the substitution given in (41) to obtain

$$T_r = A^s(r_p, r_a, \Lambda, s) \int_{-1}^1 \frac{V_t^s(x)}{\sqrt{V_r^s(x)}} dx, \quad (51)$$

$$\Delta\phi = B^s(r_p, r_a, \Lambda, s) \int_{-1}^1 \frac{V_\phi^s(x)}{\sqrt{V_r^s(x)}} dx, \quad (52)$$

where $V_t^s(x)$ and $V_\phi^s(x)$ are rational functions whose de-

nominators have no zeros in the integration interval and

$$V_r^s(x) = (1-x^2)(1+k_1x)(1+k_2x)(1+k_3x)(1+k_4x) \quad (53)$$

$$\times (1+k_5x)(1+k_6x)(x-(a_I+ib_I))(x-(a_I-ib_I)) \quad (54)$$

with

$$\begin{aligned} k_1 &= \frac{r_a - r_p}{r_a + r_p}, \\ k_2 &= \frac{r_a - r_p}{(r_a - r_1) + (r_p - r_1)}, \\ k_3 &= -\frac{r_a - r_p}{(r_2 - r_a) + (r_2 - r_p)}, \\ k_4 &= \frac{r_a - r_p}{(r_a - r_\alpha) + (r_p - r_\alpha)}, \\ k_5 &= \frac{r_a - r_p}{(r_a - r_\beta) + (r_p - r_\beta)}, \\ k_6 &= \frac{r_a - r_p}{(r_a - r_\gamma) + (r_p - r_\gamma)}, \end{aligned}$$

which satisfy $0 \leq k_6 \leq k_5 \leq k_4 \leq k_1 \leq k_2 \leq 1$ and $-1 \leq k_3 \leq 0$. As in the non-spinning case, we use Sochnev's method for evaluating these integrals near the separatrices, see the Appendix.

In Fig. 6 plots of the isofrequency pairing phenomenon for particles with two different spin values (0.1, -0.1) moving in the same Schwarzschild-de Sitter spacetime with $\Lambda = 0.0005$ are shown. The qualitative shape of the region of bound motion is similar to that of the non-spinning particle. The quantitative differences become apparent in the characteristic features of bound motion and its boundaries. Some basic facts that we have already seen in the (p, e) -diagram are obvious, such as the shifts of the maximal eccentricity, of the ISCO and of the OSCO. However, what interests us is the impact on the domain where isofrequency pairing occurs and the question of whether further degeneracies due to the spin emerge.

First, we qualitatively compare the size of the region where isofrequent orbits exist. It can be characterized by the azimuthal frequency at the ISCO (OSCO) and the one at the intersection of the COD line with the horizontal axis. Only orbits having an azimuthal frequency within this range do have isofrequent partners. The size of the allowed frequency interval decreases if the spin is chosen to be negative and increases if the spin value is positive. Although the region shrinks for negative spin it will never completely vanish as long as bound motion exists. Therefore, the spin does not destroy this degeneracy in the fundamental frequencies of the orbital motion.

Next, we compare the evolution of the maximal radial frequency for different spin values in Fig. 7. We notice immediately the shift of the entire curve closer to the center for positive spin and further away for negative spin values. This coincides with the trend of the shifts of

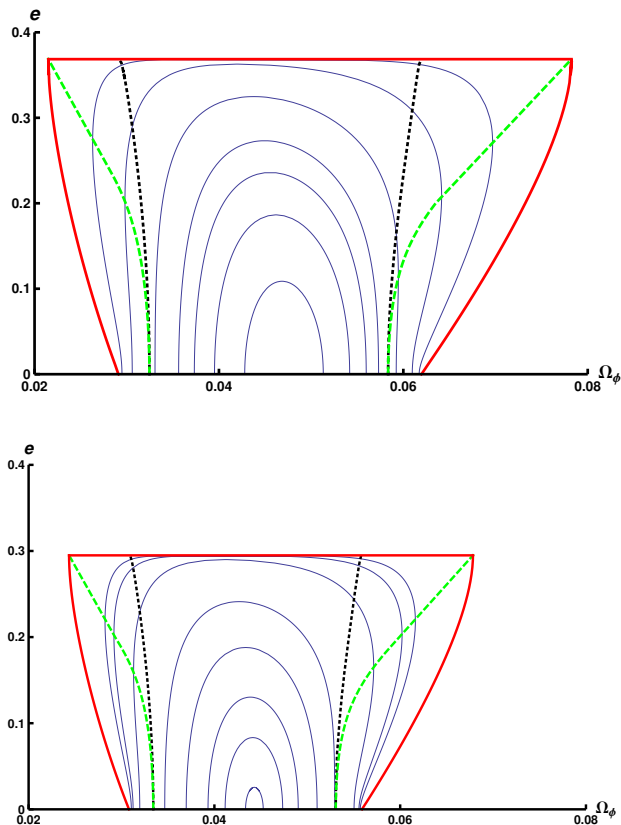


Figure 6: The figure depicts the phenomenon of isofrequency pairing for bound orbits in the (Ω_ϕ, e) -plane for a fixed $\Lambda = 0.0005$. The upper figure shows the characteristics for $s = 0.1$ and the lower one corresponds to $s = -0.1$. The thick (red) boundary lines correspond to the separatrices and confine the region of bound motion. The (blue) solid lines inside these regions correspond to constant values of Ω_r . The (green) dashed line represents the singular curve, i.e. the locus where the Jacobian determinant of the transformation from (p, e) to (Ω_r, Ω_ϕ) vanishes. The Circular Orbit Duals (COD) marking the boundaries of the domains where isofrequency pairing occur are shown by the black dotted lines.

the ISCO and OSCO. We also see the spin dependence of the value for Ω_r^{\max} for $\Lambda = 0$ (bold dots). More generally, if we choose a value for Ω_r^{\max} on the vertical axis and determine the intersection points with the three curves not only the position differs but also the corresponding Λ is not the same for the different systems.

We will now investigate if the spin induces a further degeneracy in the sense that isofrequency pairs with different spin values may have the same frequencies. We can deduce this from Fig. 6. Choose a line of constant radial frequency that lies in the isofrequency range. Then draw a line of constant azimuthal frequency that corresponds to a circular orbit located outside the range between the ISCO and the OSCO and mark the two intersection points. We know from the analysis of Ω_r^{\max} that the maximal radial frequency increases with positive spin and decreases with negative spin, keeping the cosmolog-

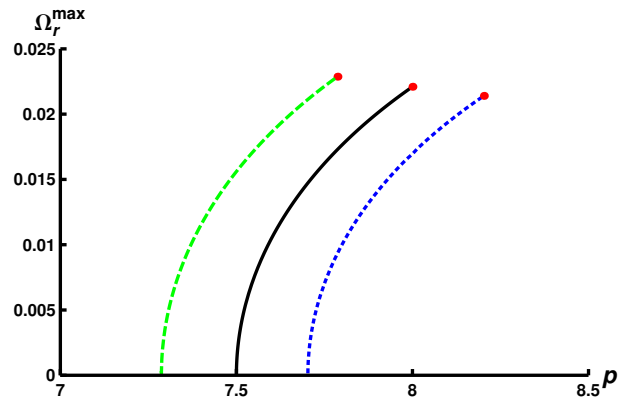


Figure 7: The figure shows the change of Ω_r^{\max} in value as well as in position from the center when the value of Λ is varied. The (red) dots mark the Schwarzschild case with $\Lambda = 0$. Along each curve Λ increases up to its maximal value when Ω_r^{\max} vanishes. The black solid curve corresponds to $s = 0$, the (green) dashed one to $s = 0.1$ and the (blue) dotted one to $s = -0.1$.

ical constant fixed. Now, imagine the line of constant Ω_r shrinking and spreading slowly for small negative and positive values for the spin parameter, respectively. The two intersection points will diverge for positive spin and approach one another for negative spin leading to six different orbits that have different eccentricities. For example, if the initial intersection points belong to a non-spinning particle and the spin is slightly changed to positive or negative values, there exist infinitely many physically distinct pairs of orbits having the same frequencies but different spin values. Even the spin direction is different in this example. If we allow both the cosmological constant and the spin parameter to vary we get two-parameter families of isofrequency pairs with the same frequencies, parametrized by (Λ, s) .

4. CONCLUSIONS AND OUTLOOK

In this work we investigated the characteristics of isofrequency pairing for both geodesic motion of a test-particle and the non-geodesic motion of a spinning test-particle moving in the equatorial plane of Schwarzschild-de Sitter spacetime. In contrast to the case without a cosmological constant, there exist *two* regions in the domain of bound orbits where isofrequency pairing occurs. More precisely, it is not only the strong field regime that exhibits such a feature but also a region close to the outermost stable circular orbit. This is associated with a greater variety of zoom-whirl orbits than in the case without a cosmological constant: There are now not only orbits that whirl near the periastron but also orbits that whirl near the apastron.

Generally, adding a cosmological constant and/or the spin leads to the emergence of additional degeneracies in the frequencies. This occurs already for arbitrarily small

values of the cosmological constant and the spin. At least in principle, this additional degeneracy is of relevance in view of gravitational wave data analysis. Here we may think of an EMRI which, among all possible gravitational wave sources, is the closest physical realization of the dynamical system considered in this paper. Whenever isofrequency pairing occurs, knowledge of the fundamental frequencies alone does not determine the shape of the orbit, i.e., additional information on the spectrum has to be taken into account.

The most obvious plan for follow-up work would be to consider more general spacetimes, such as the Kerr-deSitter-NUT... spacetime. In addition, there are several other avenues for future studies on isofrequency pairing which we would like to mention briefly.

From a theoretical point of view isofrequency pairing is of relevance in view of perturbation techniques. For example, in order to use KAM theory for perturbed integrable systems, certain non-degeneracy conditions have to be satisfied. The simplest version of these non-degeneracy conditions is obviously violated if there is a degeneracy in the frequencies such that other, more complex or more restrictive, conditions have to be tested. To mention another example, the feature of isofrequency pairing and the occurrence of a singular curve can be used to compare different approaches to the general relativistic two-body problem, as it was already mentioned in [2]. Methods such as the effective one-body approach or the post-Newtonian approximation can profit from the isofrequency pairing and its related characteristics.

Also from a theoretical point of view, it is an interesting question to ask if there are spacetimes where three or more orbits with the same frequencies exist. In all examples treated so far there are only isofrequency *pairs*. (Here we are referring to the situation that all the parameters of the dynamical system have been fixed which, for the cases treated in this paper, means fixing Λ and s .) As an attempt to find a candidate for isofrequency triples one could start with a Bertrand spacetime and perturb it a little bit. Bertrand spacetimes, which were introduced in [41], are spherically symmetric and static spacetimes in which the ratio of the radial frequency and the azimuthal frequency is a constant rational number q for all bound orbits, so they show the same total degeneracy of the frequencies as the Kepler problem but now with $q \neq 1$. We are planning to search for isofrequency triples etc. in future work.

Acknowledgments

We gratefully acknowledge support from the Deutsche Forschungsgemeinschaft within the Research Training Group 1620 “Models of Gravity” and from the “Centre for Quantum Engineering and Space-Time Research (QUEST)”. VP was financially supported by Deutsche Forschungsgemeinschaft, Grant No. LA 905/14-1.

Appendix

Approximation of hyperelliptic Integrals

In this section we briefly describe how we use the approximation scheme for hyperelliptic integrals developed by Sochnev [35]. He based the method on the approximation of irrational functions by rational ones. In particular, the irrational function $c = \sqrt[m]{c_1 c_2 \dots c_m}$ can be approximated by the sequences $\{a_n\}$ and $\{b_n\}$ which are defined iteratively by

$$a_1 = \frac{c_1 + c_2 + \dots + c_m}{m}, \quad b_1 = \frac{c_1 c_2 \dots c_m}{a_1^{m-1}}, \quad (55)$$

and

$$a_{n+1} = \frac{(m-1)a_n + b_n}{m}, \quad b_{n+1} = \frac{a_n^{m-1} b_n}{a_{n+1}^{m-1}} \quad (56)$$

for $n \geq 1$. While $\{a_n\}$ approaches c from above, $\{b_n\}$ comes from below, i.e. $a_1 > a_2 > \dots > a_n > c > b_n > \dots > b_2 > b_1$, and their common limit for $n \rightarrow \infty$ is c .

Let us consider a specific example related to our problem of hyperelliptic integrals. The irrational function $\sqrt[m]{1+kx}$ with $|k| < 1$ is finite for $-1 < x < 1$. (These boundaries become important when we consider the boundaries of the integrals.) Therefore, we can approximate this function by choosing $\sqrt[m]{1+kx} = \sqrt[m]{c_1 c_2 \dots c_m}$ with $c_1 = 1+kx$ and $c_2 = c_3 = \dots = c_m = 1$ and evaluating the sequences $\{a_n\}$ and $\{b_n\}$ within the defined range of x . In this way we approximate our irrational function by rational ones.

This method can be used for evaluating our hyperelliptic integrals (42), (43) where $m = 2$. To that end we have to approximate the function $\sqrt{V_r(x)}$ where $V_r(x)$ is given by (44). If the absolute values of the k factors are far away from one, the procedure goes like this: First, we extract the factor $(1-x^2)$ out of the radicand, arrange the k factors in decreasing order in their absolute values and group positive and negative ks . Then we form subgroups with $m = 2$ elements within each group where we supplement a factor of one when there are less than $m = 2$ elements in the subgroups, i.e.

$$\sqrt{V_r(x)} = \sqrt{1-x^2} \times \sqrt{(1-k_3x)(1+k_1x)} \sqrt{(1+k_2x) \cdot 1} \sqrt{(1+k_4x) \cdot 1} \quad (57)$$

Now we are able to compute the approximating sequences $\{a_n\}$ and $\{b_n\}$ for each subgroup up to arbitrarily high order in n , always resulting in a rational function. Consequently, the integral that has to be solved can be approximated by integrals of the form

$$\int_{-1}^1 R(x, \sqrt{1-x^2}) dx$$

where $R(x, \sqrt{1-x^2})$ denotes a rational function of x and $\sqrt{1-x^2}$. Using any of the three Euler substitutions or

elementary transformations which rearrange the form of the integral into tabulated ones, it is possible to solve the integral in terms of elementary functions.

This gives a good approximation scheme as long as the absolute values of all k s are far away from one. However, we are interested in frequencies close to the separatrices corresponding to absolute values close to one for either k_3 or k_4 . Luckily, only a few modifications to the procedure are necessary to adapt it to this case.

To begin with the integrals in (42) and (43) are divided into two integrals, where one runs from -1 to 0 and the other from 0 to 1 . Then, it is not the factor $(1-x^2)$ that is extracted. Consider

$$(1-x)(1+x)(1+k_3x)(1+k_1x)(1+k_2x)(1+k_4x)$$

where the k factors are already arranged in decreasing order in their absolute values and $(1-x^2)$ is rewritten as $(1+x)(1-x)$. In the first integral (from -1 to 0) the product $(1+x)(1+k_3x)$ is taken out where k_3 is the greatest of the positive coefficients k_i leading to

$$\int_{-1}^0 \frac{dx}{\sqrt{(1+x)(1+k_3x)}} \mathcal{A}(x, k_1, k_2, k_4)$$

where $\mathcal{A}(x, k_1, k_2, k_3) = \sqrt{(1+k_1x)(1+k_2x)(1-x)(1+k_4x)}$ has to be approximated by the same procedure as explained above. The second integral (from 0 to 1) is rearranged in such a way that it yields

$$\int_0^1 \frac{dx}{\sqrt{(1-x)(1+k_4x)}} \mathcal{B}(x, k_1, k_2, k_3)$$

with $\mathcal{B}(x, k_1, k_2, k_3) = \sqrt{(1+x)(1+k_3x)(1+k_1x)(1+k_2x)}$. Here, the factor $(1+k_4x)$ is pulled out together with $(1-x)$ because k_4 is the greatest of the negative coefficients k_i . Again, the remaining function is approximated resulting in a rational function in x . Therefore we obtain for our integral an approximation of the form

$$\int_{-1}^0 \frac{R_1(x)dx}{\sqrt{(1+x)(1+k_3x)}} + \int_0^1 \frac{R_2(x)dx}{\sqrt{(1-x)(1+k_4x)}}$$

the solution of which can be found in terms of elementary functions. In order to simplify the calculations further we may apply partial fraction decompositions to each of the rational functions providing us with integrals of the form

$$\int_{-1}^0 \frac{dx}{(1+a(k_1, k_2, k_4)x)\sqrt{(1+x)(1+k_3x)}},$$

$$\int_0^1 \frac{dx}{(1+b(k_1, k_2, k_3)x)\sqrt{(1-x)(1+k_4x)}}.$$

In the spinning case, we have to evaluate the integrals (51) and (52), i.e., we have to approximate the function $\sqrt{V_r^s(x)}$ with $V_r^s(x)$ given by (53). It is convenient to treat the two non-real zeros and the real zeros separately. Since

$$\sqrt{(x-(a_I+ib_I))(x-(a_I-ib_I))}$$

is a real-valued irrational function it is possible to approximate it by Sochnev's method leading to

$$\sqrt{(x-(a_I+ib_I))(x-(a_I-ib_I))} \rightarrow$$

$$\left(\frac{r_a-r_p}{2}-a_I\right)\left(1+\frac{r_a-r_p}{r_a+r_p-2a_I}x\right)$$

in first approximation, which proves to be of sufficient accuracy for our purposes. Therewith, the remaining terms

$$\sqrt{(1-x^2)(1+k_1x)(1+k_2x)(1+k_3x)(1+k_4x)(1+k_5x)(1+k_6x)}$$

can be approximated analogously to the non-spinning case. Here, close to the separatrices either k_2 or $-k_3$ approaches 1, and the approximation only contains elementary integrals which, after partial fraction decomposition, reduce to integrals of the form

$$\int_{-1}^0 \frac{dx}{(1+a_s(k_1, k_2, k_4)x)\sqrt{(1+x)(1+k_2x)}},$$

$$\int_0^1 \frac{dx}{(1+b_s(k_1, k_2, k_3)x)\sqrt{(1-x)(1+k_3x)}}. \quad (58)$$

-
- [1] L. Barack and N. Sago, *Phys. Rev. D* **83**, 084023 (2011).
 - [2] N. Warburton, L. Barack, N. Sago, *Phys. Rev. D* **87**, 084012 (2013).
 - [3] S. Shaymatov, F. Atamurotov, B. Ahmedov, *Astrophys. Space Sci.* **350**, 413 (2014).
 - [4] Z. Stuchlík, *Acta Physica Slovaca* **49**, 319 (1999).
 - [5] M. Mortazavimanesh and M. Mohseni, *Gen. Rel. Grav.* **41**, 2697 (2009).
 - [6] Y. N. Obukhov, D. Puetzfeld, *Phys. Rev. D* **83**, 044024 (2011).
 - [7] Z. Stuchlík and S. Hledík, *Phys. Rev. D* **60**, 044006 (1999).
 - [8] Z. Stuchlík and J. Kovář, in *Proceedings of RAGtime 8/9: Workshops on black holes and neutron stars*, edited by

- S. Hledík and Z. Stuchlík (Silesian University of Opava, 2007) 417.
- [9] E. Hackmann and C. Lämmerzahl, *Phys. Rev. D* **78**, 024035 (2008).
- [10] M. Mathisson, *Acta Phys. Polonica* **6**, 163 (1937).
- [11] A. Papapetrou, *Proc. R. Soc. London Ser. A* **209**, 248 (1951).
- [12] W. G. Dixon, *Proc. R. Soc. London Ser. A* **314**, 499 (1970); *Proc. R. Soc. London Ser. A* **319**, 509 (1970); *Proc. R. Soc. London Ser. A* **277**, 59 (1974).
- [13] O. Semerák, *Mon. Not. R. Astron. S.* **308**, 863 (1999).
- [14] K. Kyrian, and O. Semerák, *Mon. Not. R. Astron. S.* **382**, 1922 (2007).
- [15] L. F. Costa, C. Herdeiro, J. Natario and M. Zilhão, *Phys.*

- Rev. D* **85**, 024001 (2012).
- [16] G. Lukes-Gerakopoulos, J. Seyrich, D. Kunst, *Phys. Rev. D* **90**, 104019 (2014).
 - [17] C. Möller, *Annales de l'I. H. P.* **11**, 251 (1949).
 - [18] T. D. Newton and E. P. Wigner, *Rev. Mod. Phys.* **21**, 400 (1949).
 - [19] E. Corinaldesi and A. Papapetrou, *Proc. R. Soc. London Ser. A* **209**, 259 (1951).
 - [20] F. A. E. Pirani, *Acta Phys. Polonica* **15**, 389 (1956).
 - [21] W. Tulczyjew, *Acta Phys. Polonica* **18**, 393 (1959).
 - [22] I. Bailey, and W. Israel, *Commun. Math. Phys.* **42**, 65 (1975).
 - [23] J. Steinhoff, G. Schäfer, and S. Hergt, *Phys. Rev. D* **77**, 104018 (2008).
 - [24] J. Steinhoff, *Annal. Phys* **523**, 296 (2011).
 - [25] R. Plyatsko, M. Fenyk, *Phys. Rev. D* **85**, 104023 (2012).
 - [26] R. Plyatsko, M. Fenyk, *Phys. Rev. D* **87**, 044019 (2013).
 - [27] E. Hackmann, C. Lämmerzahl, Y. N. Obukhov, D. Puetzfeld, I. Schaffer, *Phys. Rev. D* **90**, 064035 (2014).
 - [28] J. Steinhoff, and D. Puetzfeld, D., *Phys. Rev. D* **86**, 044033 (2012).
 - [29] S. Suzuki and K. Maeda, *Phys. Rev. D* **55**, 4848 (1997).
 - [30] M. D. Hartl, *Phys. Rev. D* **67**, 024005 (2003).
 - [31] M. D. Hartl, *Phys. Rev. D* **67**, 104023 (2003).
 - [32] C. Verhaaren, E. W. Hirschmann, *Phys. Rev. D* **81**, 124034 (2010).
 - [33] W. Rindler, *Relativity* (Oxford University Press, Oxford, 2001).
 - [34] C. Cutler, D. Kennefick and E. Poisson, *Phys. Rev. D* **50**, 3816 (1994).
 - [35] A. Ya. Sochnev, *Uk. Math. Journal* **20**, 442 (1968).
 - [36] P.J.E. Peebles and B. Ratra, *Rev. Mod. Phys.* **75**, 559, (2003).
 - [37] M. Saijo, K. Maeda, M. Shibata and Y. Mino, *Phys. Rev. D* **58**, 064005 (1998).
 - [38] M. Favata, *Phys. Rev. D* **83**, 024028 (2011).
 - [39] T. Tanaka, Y. Mino, M. Sasaki and M. Shibata, *Phys. Rev. D* **54**, 3762 (1996).
 - [40] S. Suzuki and K. Maeda, *Phys. Rev. D* **58**, 023005 (1998).
 - [41] V. Perlick, *Class. Quant. Grav.* **9**, 1009 (1992).
 - [42] J. Levin and G. Perez-Giz, *Phys. Rev. D* **79**, 124013 (2009).
 - [43] R. O'Shaughnessy, *Phys. Rev. D* **67**, 044004 (2003).
 - [44] K. Glampedakis, D. Kennefick, *Phys. Rev. D* **66**, 044002 (2002).
 - [45] J. Levin, R. O'Reilly and E. J. Copeland, *Phys. Rev. D* **62**, 024023 (2000).